International Journal of Nanoelectronics and Materials
Volume 13 (Special Issue) May 2020 [295-304]

Prediction Effects on Internal Resonance Wave of Metallic Conductive Ink in Rotational Motion Behaviour

Mohd Azli Salim[1,2*], Feng Dai[3], Adzni Md. Saad[2], Nor Azmmi Masripan[2], Andrey Nikolayevich Dmitriev[4], Azmi Naroh[5], Ghazali Omar[1,2] and Mohd Zaid Akop[2]

[1]*Advanced Manufacturing Centre, Universiti Teknikal Malaysia Melaka, Hang Tuah Jaya, 76100 Durian Tunggal, Melaka, Malaysia.*
[2]*Fakulti Kejuruteraan Mekanikal, Universiti Teknikal Malaysia Melaka, Hang Tuah Jaya, 76100 Durian Tunggal, Melaka, Malaysia.*
[3]*China Railway Eryuan Engineering Group Co., Ltd, No. 3 Tongjin Road, Chengdu, China.*
[4]*Institute of Metallurgy of Ural Branch of Russian Academy of Sciences, Ural Federal University, Russia.*
[5]*Jabatan Kejuruteraan Mekanikal, Politeknik Ungku Omar, Jalan Raja Musa Mahadi, 31400 Ipoh, Perak, Malaysia.*

ABSTRACT

This paper represents the effects on internal resonance wave of metallic conductive ink in rotational motion behaviour. The internal resonance metallic conductive ink model is developed using the wave propagation approach. There are two equations derived from this which are impedance and stiffness. Based on these two equations, the multi-body metallic conductive ink model has been successfully derived in order to observe the behaviour of internal resonance, when force is applied at both ends of the model. The internal resonance wave was predicted, and the results have been recorded, and finally, the location of the internal resonance was identified. The maximum level of frequency recorded was at 10 kHz. It is believed that these results can be used in future analysis of metallic conductive ink in order to evaluate and investigate the range of the conductivity of ink with predictive method.

Keywords: Conductive Ink, Internal Resonance, Rotational Behavior.

1. INTRODUCTION

Recently, many electronic products are being made using the micron size. [1]. This is because of the progressive advancement of technology in the future that will replace the current electronic packaging, rigid electronic and super scale packaging. Therefore, the revolution of micron-size technology is needed for tomorrow's technology [2-3].

Metallic conductive ink (MCI) has the capability to produce electrical conductivity in small value. Many conductive inks have been made by metal materials because the materials itself have high conductivity coefficients. In addition, the ink is capable of expanding, and it allows many applications to be used as a secondary circuit to operate the system [4]. However, until today, the level of conductivity of the ink can only be investigated and evaluated using an experimental approach [5]. Based on this approach, many efforts and financing have been used by engineers and researchers [6-7].

In this paper, the MCI model was developed using the modelling estimation and prediction approach for non-linear technique. In this study, the model was represented as a baseline MCI model with conductivity range. The conductivity material basically has been blended together

*Corresponding Author: *azli@utem.edu.my*

with polymer in order to have one shape. This prediction technique will be used in order to check and examine the range of conductivity of the MCI model.

2. MATERIAL AND METHODS

Consider a uniform stretchable conductive ink (SCI) model having L length subjected to a longitudinal direction of force as shown in Figure 1.

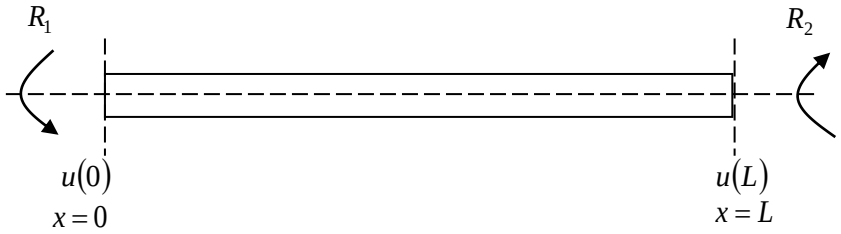

Figure 1. The uniform stretchable conductive ink model having *L* length subjected to a longitudinal direction of force.

The general equation of motion for the SCI model can be represented as

$$c_r^2 \frac{\partial^2 u(x,t)}{\partial^2 x} = \frac{\partial^2 u(x,t)}{\partial^2 t} \tag{1}$$

where $c_r = \sqrt{G/\rho}$ and G is complex shear modulus and ρ is density.

By applying the forces at both ends of the SCI model, it generates the harmonic reaction and Eq. (1) produces negative and positive going wave in the microstructure reaction, and it is represented in Figure 2 and the new equation is illustrated in Eq. (2).

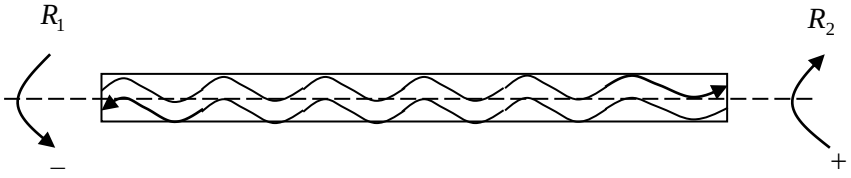

Figure 2. Forces are applied at both ends of the stretchable conductive ink model and it produces negative and positive going wave in microstructure reaction

$$u(x,t) = u(x)e^{j\omega t} = \left(A_r e^{jk_r x} + B_r e^{-jk_r x}\right)e^{j\omega t} \tag{2}$$

where A_r and B_r are complex wave amplitudes.

For rotational of SCI model, shear wavenumber equation can be represented as

$$k_r = \frac{\omega}{c_r} = \sqrt{\frac{\rho}{G}} \cdot \omega \tag{3}$$

At point impedance, it is said that the SCI model at each end are equal due to symmetry. Based on this theoretical understanding, it becomes

$$Z_{11} = \left.\frac{R_1}{\dot{u}(0)}\right|_{\dot{u}(L)=0}$$

and

$$Z_{22} = \left.\frac{R_2}{\dot{u}(L)}\right|_{\dot{u}(0)=0} \tag{4}$$

By applying Hooke Law at $x = 0$, the previous equation can be written as

$$jk_r A_r = jk_r B_r = -\frac{R_1}{\kappa_r}$$

and

$$A_r - B_r = -\frac{R_1}{\kappa_r jk_r} \tag{5}$$

According to Eq. (5), the new equation can be given as

$$\frac{\partial u(0)}{\partial x} = -\frac{R_1}{\kappa_r} \tag{6}$$

where $\kappa_r = G \cdot J_r$, J_r is polar second moment of area of SCI model based on rectangular shape.

At boundary condition $x = L$, the equation become

$$\dot{u}(L) = j\omega u(L) = 0 \tag{7}$$

By substituting Eq. (2) into Eq. (6) and Eq. (7), and letting the boundary condition at $x = 0$ and $x = L$, Eq. (6) can be rearranged as

$$A_r\left(1 + e^{2jk_r L}\right) = -\frac{R_1}{\kappa_r jk_r} \tag{8}$$

Then, it is followed by Eq. (7),

$$A_r e^{jk_r L} + B_r e^{-jk_r L} = 0 \tag{9}$$

By simplifying Eq. (9), the equation becomes

$$A_r e^{2jk_r L} + B_r = 0 \tag{10}$$

Finally, the equations become

$$A_r = -\frac{R_1}{jk_r \kappa_r} \cdot \frac{1}{e^{2jk_r L} + 1}$$

and

$$B_r = \frac{R_1}{jk_r\kappa_r} \cdot \frac{e^{2jk_rL}}{e^{2jk_rL}+1} \tag{11}$$

By substituting Eq. (11) into Eq. (2) and letting boundary condition at $x = 0$, so

$$u(0) = \frac{R_1}{jk_r\kappa_r} \cdot \frac{e^{2jk_rL}-1}{e^{2jk_rL}+1} = \frac{R_1}{k_r\kappa_r} \cdot \tan(k_rL) \tag{12}$$

From Eq. (12), differentiate the equation into time and it gives

$$Z_{11} = \frac{R_1}{\dot{u}(0)} = \frac{R_1}{j\omega u(0)} = \frac{k_r\kappa_r}{j\omega\tan(k_rL)} \tag{13}$$

For transfer impedance, it is said that the SCI model at each end are equal to reciprocity [8 -9]. According to this statement, the impedance equation-becomes

$$Z_{12} = \left.\frac{R_1}{\dot{u}(L)}\right|_{\dot{u}(0)=0}$$

and

$$Z_{21} = \left.\frac{R_2}{\dot{u}(0)}\right|_{\dot{u}(L)=0} \tag{14}$$

For $x = 0$ and by applying Hooke Law again, it is still valid. Then, for Z_{12} it becomes

$$\dot{u}(0) = j\omega u(0) = 0 \tag{15}$$

By substituting Eq. (2) into Eq. (6) and Eq. (15) by letting boundary condition at $x = 0$, the new equation becomes

$$A = -\frac{R_1}{2jk_r\kappa_r}$$

and

$$B = \frac{R_1}{2jk_r\kappa_r} \tag{16}$$

Insert Eq. (16) into Eq. (2) and letting boundary condition at $x = L$, the equation becomes

$$u(L) = \frac{R_1}{2jk_r\kappa_r} \cdot \left(e^{-jk_rL} - e^{jk_rL}\right) = -\frac{R_1}{k_r\kappa_r} \cdot \sin(k_rL) \tag{17}$$

Take Eq. (17) and differentiate respect to time and the new equation becomes

$$Z_{12} = \frac{R_1}{\dot{u}(L)} = \frac{R_1}{j\omega u(L)} = -\frac{k_r \kappa_r}{j\omega \sin(k_r L)} \tag{18}$$

The impedance matrix SCI model matrix is

$$Z = \begin{bmatrix} Z_{11} & Z_{12} \\ Z_{21} & Z_{22} \end{bmatrix} = \frac{k_r \kappa_r}{j\omega \sin(k_r L)} \cdot \begin{bmatrix} \cos(k_r L) & -1 \\ -1 & \cos(k_r L) \end{bmatrix} \tag{19}$$

By substituting k_r and κ_r for rotational internal resonance of SCI model, the equation becomes

$$Z = \begin{bmatrix} Z_{11} & Z_{12} \\ Z_{21} & Z_{22} \end{bmatrix} = \frac{J_r \sqrt{G \cdot \rho}}{j \sin(k_r L)} \cdot \begin{bmatrix} \cos(k_r L) & -1 \\ -1 & \cos(k_r L) \end{bmatrix} \tag{20}$$

By simplifying Eq. (20),

$$Z_{11} = \frac{J_r \sqrt{G \cdot \rho}}{j \sin(k_r L)} \cdot \cos(k_s L) = \frac{J_r \sqrt{G \cdot \rho} \cdot \cos(k_r L)}{j \sin(k_r L)} = -jJ_r \sqrt{G \cdot \rho} \cdot \cot(k_r L) \tag{21}$$

$$Z_{12} = \frac{J_r \sqrt{G \cdot \rho}}{j \sin(k_r L)} \cdot -1 = \frac{jJ_r \sqrt{G \cdot \rho}}{\sin(k_r L)} \tag{22}$$

$$Z_{21} = \frac{J_r \sqrt{G \cdot \rho}}{j \sin(k_r L)} \cdot -1 = \frac{jJ_r \sqrt{G \cdot \rho}}{\sin(k_r L)} \tag{23}$$

and

$$Z_{22} = \frac{J_r \sqrt{G \cdot \rho}}{j \sin(k_r L)} \cdot \cos(k_r L) = \frac{J_r \sqrt{G \cdot \rho} \cdot \cos(k_r L)}{j \sin(k_r L)} = -jJ_r \sqrt{G \cdot \rho} \cdot \cot(k_r L) \tag{24}$$

In matrix form for impedance of SCI model can be written as

$$Z = \begin{bmatrix} Z_{11} & Z_{12} \\ Z_{21} & Z_{22} \end{bmatrix} = \begin{bmatrix} -jJ_r \sqrt{G \cdot \rho} \cdot \cot(k_r L) & \frac{jJ_r \sqrt{G \cdot \rho}}{\sin(k_r L)} \\ \frac{jJ_r \sqrt{G \cdot \rho}}{\sin(k_r L)} & -jJ_r \sqrt{G \cdot \rho} \cdot \cot(k_r L) \end{bmatrix} \tag{25}$$

Finally, the relationship between the equations in Eq. (21) to Eq. (24) can be simplified as below.

$$Z_{11} = Z_{22} = -jJ_r \sqrt{G \cdot \rho} \cdot \cot(k_r L)$$

and

$$Z_{12} = Z_{21} = \frac{jJ_r \sqrt{G \cdot \rho}}{\sin(k_r L)} \tag{26}$$

Impedance equation also can be written in stiffness domain for SCI model. In stiffness, the equation becomes

$$K_{11} = K_{22} = \frac{R_1}{X_1} = \frac{GA}{h}\left(\frac{k_r h}{\tan(k_r h)}\right)$$

and

$$K_{12} = K_{21} = \frac{R_2}{X_1} = \frac{GA}{h}\left(\frac{k_r h}{\sin(k_r h)}\right) \tag{27}$$

where h is the thickness of the sample and A is a cross sectional area for the hybrid vibration control model.

According to Eq. (27), it can only be used for a singular body. In the multi-body system, both equations need to be arranged and matrix form is used. In singular body, the equation shown in Eq. (28).

$$\text{One DOF for SCI model} = \begin{bmatrix} \overset{(1)}{K}_{(11)} & \overset{(1)}{K}_{(12)} \\ \overset{(1)}{K}_{(21)} & \overset{(1)}{K}_{(22)} \end{bmatrix} \tag{28}$$

where $\overset{(1)}{K}_{11}$ refers to the stiffness for element 1 at coordinate (1,1), $\overset{(1)}{K}_{12}$ refers to the stiffness for element 1 at coordinate (1,2), $\overset{(1)}{K}_{21}$ refers to the stiffness for element 1 at coordinate (2,1) and $\overset{(1)}{K}_{22}$ refers to the stiffness for element 1 at coordinate (2,2).

The coordinate can be plotted in the uniform SCI model and is shown in Figure 3.

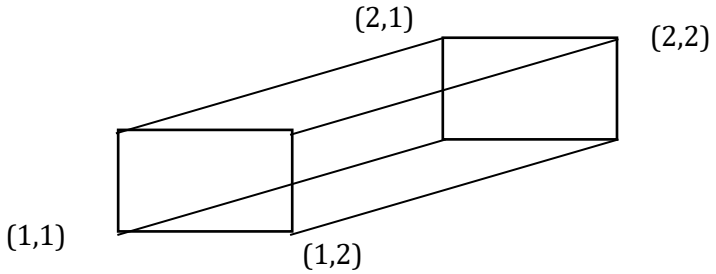

Figure 3. Coordinate for the stretchable conductive ink model.

Based on the figure, the multi-body system for the SCI model, can be written in the matrix form. Additionally, the two, three and four bodies of hybrid control vibration system equation can be represented as

Two bodies for SCI model

$$= \begin{bmatrix} \overset{(1)}{K}_{(11)} & \overset{(1)}{K}_{(12)} \\ \overset{(1)}{K}_{(21)} & \overset{(1)}{K}_{(22)} \end{bmatrix} + \begin{bmatrix} \overset{(2)}{K}_{(11)} & \overset{(2)}{K}_{(12)} \\ \overset{(2)}{K}_{(21)} & \overset{(2)}{K}_{(22)} \end{bmatrix} = \begin{bmatrix} \overset{(1)}{K}_{(11)} + \overset{(2)}{K}_{(11)} & \overset{(1)}{K}_{(12)} + \overset{(2)}{K}_{(12)} \\ \overset{(1)}{K}_{(21)} + \overset{(2)}{K}_{(21)} & \overset{(1)}{K}_{(22)} + \overset{(2)}{K}_{(22)} \end{bmatrix} \tag{29}$$

Three bodies for SCI model

$$=\begin{bmatrix} {}^{(1)}K_{(11)} & {}^{(1)}K_{(12)} \\ {}^{(1)}K_{(21)} & {}^{(1)}K_{(22)} \end{bmatrix}+\begin{bmatrix} {}^{(2)}K_{(11)} & {}^{(2)}K_{(12)} \\ {}^{(2)}K_{(21)} & {}^{(2)}K_{(22)} \end{bmatrix}+\begin{bmatrix} {}^{(3)}K_{(11)} & {}^{(3)}K_{(12)} \\ {}^{(3)}K_{(21)} & {}^{(3)}K_{(22)} \end{bmatrix}=\begin{bmatrix} {}^{(1)}K_{(11)}+{}^{(2)}K_{(11)}+{}^{(3)}K_{(11)} & {}^{(1)}K_{(12)}+{}^{(2)}K_{(12)}+{}^{(3)}K_{(12)} \\ {}^{(1)}K_{(21)}+{}^{(2)}K_{(21)}+{}^{(3)}K_{(21)} & {}^{(1)}K_{(22)}+{}^{(2)}K_{(22)}+{}^{(3)}K_{(22)} \end{bmatrix} \tag{30}$$

Four bodies for SCI model

$$=\begin{bmatrix} {}^{(1)}K_{(11)} & {}^{(1)}K_{(12)} \\ {}^{(1)}K_{(21)} & {}^{(1)}K_{(22)} \end{bmatrix}+\begin{bmatrix} {}^{(2)}K_{(11)} & {}^{(2)}K_{(12)} \\ {}^{(2)}K_{(21)} & {}^{(2)}K_{(22)} \end{bmatrix}+\begin{bmatrix} {}^{(3)}K_{(11)} & {}^{(3)}K_{(12)} \\ {}^{(3)}K_{(21)} & {}^{(3)}K_{(22)} \end{bmatrix}.+\begin{bmatrix} {}^{(4)}K_{(11)} & {}^{(4)}K_{(12)} \\ {}^{(4)}K_{(21)} & {}^{(4)}K_{(22)} \end{bmatrix}\ldots \tag{31}$$

$$\ldots=\begin{bmatrix} {}^{(1)}K_{(11)}+{}^{(2)}K_{(11)}+{}^{(3)}K_{(11)}+{}^{(4)}K_{(11)} & {}^{(1)}K_{(12)}+{}^{(2)}K_{(12)}+{}^{(3)}K_{(12)}+{}^{(4)}K_{(12)} \\ {}^{(1)}K_{(21)}+{}^{(2)}K_{(21)}+{}^{(3)}K_{(21)}+{}^{(4)}K_{(21)} & {}^{(1)}K_{(22)}+{}^{(2)}K_{(22)}+{}^{(3)}K_{(22)}+{}^{(4)}K_{(22)} \end{bmatrix}$$

By following the pattern from Eq. (29) to Eq. (31), the multi-body matrix for the SCI model can be derived as

Multi-body of SCI model

$$=\begin{bmatrix} {}^{(n-(n-1))}K_{(11)} & {}^{(n-(n-1))}K_{(12)} \\ {}^{(n-(n-1))}K_{(21)} & {}^{(n-(n-1))}K_{(22)} \end{bmatrix}+\begin{bmatrix} {}^{(n-(n-2))}K_{(11)} & {}^{(n-(n-2))}K_{(12)} \\ {}^{(n-(n-2))}K_{(21)} & {}^{(n-(n-2))}K_{(22)} \end{bmatrix}+\begin{bmatrix} {}^{(n-(n-3))}K_{(11)} & {}^{(n-(n-3))}K_{(12)} \\ {}^{(n-(n-3))}K_{(21)} & {}^{(n-(n-3))}K_{(22)} \end{bmatrix}+\begin{bmatrix} {}^{(n-(n-n))}K_{(11)} & {}^{(n-(n-n))}K_{(12)} \\ {}^{(n-(n-n))}K_{(21)} & {}^{(n-(n-n))}K_{(22)} \end{bmatrix} \tag{32}$$

where n is the maximum number of bodies.

Equation (32) can be illustrated in the diagram with the length of the system being constant but divided into small parts. By doing this, the same system is presumed transferred to the multi-body of SCI model. Figure 4 shows the multi-body diagram for SCI model.

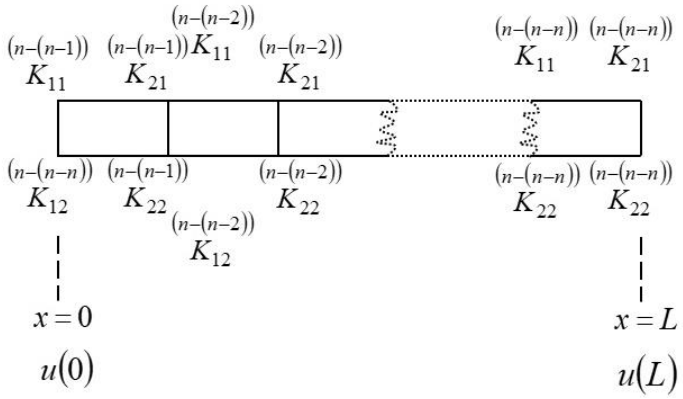

Figure 4. Multi-body diagram for SCI model.

3. RESULTS AND DISCUSSION

Internal resonance wave effects are based on many factors which depend on the materials shape, properties, radius, length, thickness and most importantly the boundary condition of the materials during tests. All these factors have effects in terms of deformation, shear, compression, elongation and many more. Wave effects are more important for stretchable and flexible materials because the static stiffness is bigger than the rigid and non-flexible materials.

Wave effects also can exchange the energy between conventional motion in the same or different direction. It occurs when the different motions in different directions interrupt the dynamic behavior and mostly affect the internal strength of the materials, and in this study, it affects the conductivity of the metallic materials itself. The internal resonances are produced by two methods which are impedance and stiffness.

In impedance, the internal resonance location is detected at the longitudinal wave direction of SCI model. Based on these four locations, the internal resonance of SCI model occurs when the frequency reaches 1 kHz and above. At this frequency range, the internal wave is generated by applying tension force and then, it fluctuates at the end of the SCI model and is called the positive wave. After reaching the end, the direction of the internal wave changes and goes back to the initial boundary and is called the negative wave feedback.

All these results are shown in Figure 5. In addition, internal resonance of the SCI model can also be plotted in stiffness and the results are shown in Figure 6.

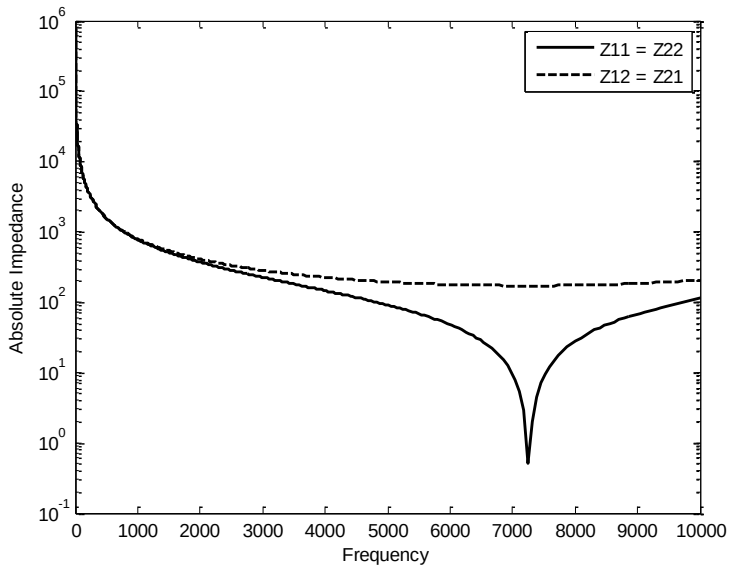

Figure 5. Impedance for stretchable conductive ink model.

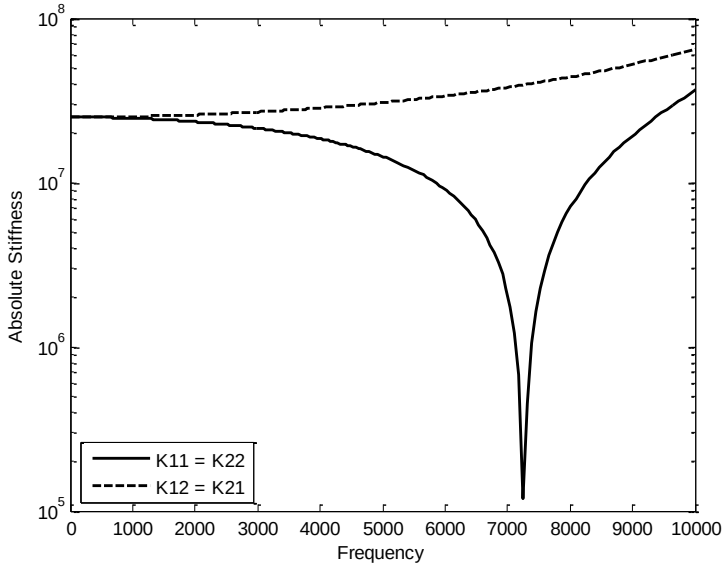

Figure 6. Stiffness for the stretchable conductive ink model.

4. CONCLUSION

This study represents the modelling estimation and prediction of the SCI model due to the internal resonance wave effect. There are two types of dynamic formulation, which are impedance and stiffness. The multi-body of the SCI model has been successfully, developed and based on the results, the internal resonance for the SCI model occurred at the same point and it was recorded at 10 kHz. One conclusion has been observed, these effects can be used to investigate and evaluate the conductivity performance of metallic based materials in the electronic packaging industry in the future.

ACKNOWLEDGEMENTS

This work has been partially supported by the grant PJP/2016/FKM-CARE/S01506 of Universiti Teknikal Malaysia Melaka (UTeM). Gratitude is also expressed to the Advanced Manufacturing Centre and the Fakulti Kejuruteraan Mekanikal, UTeM.

REFERENCES

[1] Li, Tianhua, & Hongbo Hu. Preparation and Performance of Conductive Copper Ink Based on Chemical Deoxidization. Chemical Engineering Transactions, issue **66** (2018) 31-36.

[2] Titkov, A. I., O. G. Bukhanets, R. M. Gadirov, Yu M. Yukhin, & N. Z. Lyakhov. Conductive inks for inkjet printing based on composition of nanoparticles and organic silver salt. Inorganic Materials: Applied Research **6**, 4 (2015) 375-381.

[3] Sergeev, A. S., A. R. Tameev, V. I. Zolotarevskii, & A. V. Vannikov. Electrically conductive inks based on polymer composition for inkjet printing. Inorganic Materials: Applied Research **9**, 1 (2018) 147-150.

[4] Salim, Mohd Azli., Roshidah Hamidi, & Adzni Md Saad. Development of Sheet Resistivity on Silver Nanoparticle Filled Epoxy for Electronic Packaging Devices. In 1st Colloquium Paper: Advanced Materials and Mechanical Engineering Research (CAMMER'18), Penerbit Universiti, Universiti Teknikal Malaysia Melaka **1** (2018) 1-5.

[5] Omar, G., M. A. Salim, B. R. Mizah, A. A. Kamarolzaman, & R. Nadlene. Electronic Applications of Functionalized Graphene Nanocomposites. In Functionalized Graphene Nanocomposites and their Derivatives, (2019) 245-263.
[6] Rosszainily, I. R. A., Salim, M. A., Mansor, M. R., Akop, M. Z., Putra, A., Musthafah, M. T., & Sudin, M. N. Effect of carbon black fillers on tensile stress of unvulcanized natural rubber compound. Journal of Mechanical Engineering and Sciences **10**, 2 (2016) 2043-2052.
[7] Salim, M. A., Putra, A., & Abdullah, M. A. Analysis of axial vibration in the laminated rubber-metal spring. In Advanced Materials Research **845** (2014) 46-50.
[8] Abbasi, Amirhassan, S. E. Khadem, & Saeed Bab, Vibration control of a continuous rotating shaft employing high-static low-dynamic stiffness isolators. Journal of Vibration and Control **24**, 4 (2018) 760-783.
[9] Nguyen, X. B., Komatsuzaki, T., Iwata, Y., & Asanuma, H. Modeling and semi-active fuzzy control of magnetorheological elastomer-based isolator for seismic response reduction. Mechanical Systems and Signal Processing **101** (2018) 449-466.